https://doi.org/10.5194/egusphere-2024-307
Preprint. Discussion started: 7 February 2024

The effects of orbital forcing on the East Asian Summer Monsoon for the past 450 kyr

Taiga Matsushita[1], Mariko Harada[2*], Hiroaki Ueda[3], Takeshi Nakagawa[4], Yoshimi Kubota[5], Yoshiaki Suzuki[6], Youichi Kamae[3]

[1]Graduate School of Science and Technology, University of Tsukuba, Tsukuba, Ibaraki 305-8577, Japan
[2]Department of Earth and Planetary Sciences, Tokyo Institute of Technology, Tokyo 152-8550, Japan
[3]Faculty of Life and Environmental Sciences, University of Tsukuba, Tsukuba, Ibaraki 305-8577, Japan
[4]Research Centre for Palaeoclimatology, Ritsumeikan University, Kusatsu, Fukui 525-8577, Japan
[5]Department of Geology and Paleontology, National Museum of Nature and Sciences, Tsukuba, Ibaraki 305-0005, Japan
[6]Marine Geology Research Group, National Institute of Advanced Industrial Science and Technology, Tsukuba, Ibaraki 305-8567, Japan

Correspondence to: Mariko Harada (harada.m.an@m.titech.ac.jp)

Abstract. Understanding orbital-scale changes in East Asian summer monsoon (EASM) precipitation is a fundamental issue in paleoclimate research for assessing the response of the East Asian monsoon to different climate forcings, such as insolation, ice volume, and greenhouse gases. However, owing to the inconsistencies between different proxies, the fundamental driving force for EASM variability remains controversial. In the present study, the global climate under the given insolation changes over the past 450 kyr was calculated using a climate model, Meteorological Research Institute Coupled General Circulation Model version 2.3 (MRI‑CGCM2.3). The calculated change in summer precipitation is dominated by a 20-kyr precession cycle over China, highly consistent with cave $\delta^{18}O$ records in southeast China. The proxy data from northern China (Chinese Loess Plateau) and Japan (Lake Biwa) cannot be fully explained by the calculation results, implying the importance of other forcing such as ice-sheet volume. A strong positive correlation was observed between insolation and precipitation over the coastal area of China and a negative correlation between insolation and precipitation around Japan. The results imply that the EASM is affected by the insolation intensity; however, the effect can vary between regions. The positive correlation between boreal summer insolation and precipitation over China results from the atmosphere-ocean interaction over the Indian Ocean and the western Pacific. Under intense insolation, the northern shift of the monsoon front associated with the intensification of the North Pacific subtropical high causes an increase in rainfall in the coastal area of China. The intensification of the subtropical high is caused by the integration of local wind–evaporation–sea surface temperature (WES) feedback with the Kelvin wave response to the warm Indian Ocean (IPOC mode). In contrast, the EASM intensity around Japan was affected by the strength of the North Pacific High. Under strong insolation, the North Pacific High intensified, causing a decrease in summer precipitation around Japan.

https://doi.org/10.5194/egusphere-2024-307
Preprint. Discussion started: 7 February 2024

1 Introduction

The East Asian summer monsoon (EASM) plays an essential role in the hydrological cycle over East Asia, affecting food production, water supply, and other extreme events such as floods and droughts in densely populated areas (Zhisheng et al., 2015). Understanding the variability of the EASM is crucial in assessing future climate projections (e.g., global warming) in the East Asian climate and, eventually, in human social and economic activity. Notably, investigating the long-term variation in the EASM over geological time is of fundamental importance in modern and paleo-climatology, as it enables us to reveal the mechanisms of the EASM variability under different climatic forcings.

The late Pleistocene climate, characterised by periodic changes in the Northern Hemisphere summer insolation and the high-latitude ice volume, has received considerable attention. The insolation cycle is caused by variations in three of the Earth's orbital parameters: precession (23 kyr periodicity), obliquity (41 kyr), and eccentricity (100 kyr) (Berger, 1978; Berger and Loutre, 1991). Although changes in eccentricity have a relatively small effect on insolation variability, the eccentricity cycle is considered to be an underlying cause of the 100 kyr glacial-interglacial cycle (Lisiecki and Raymo, 2005) through interaction between the climate, ice sheets, and lithosphere-asthenosphere system (Abe-Ouchi et al., 2013). These orbital and glacial factors could be the major driving forces of EASM variability during the late Pleistocene (Wang et al., 2017).

Geological records indicate that the EASM varies in phase with orbital cycles, suggesting that the EASM is affected by changes in insolation or ice volume, or both (e.g., Cheng et al., 2016; Clemens et al., 2018; G. Liu et al., 2020; Sun et al., 2006, 2015, 2019). However, the dominant cycles varied between the studies. For example, loess-paleosol records from the Chinese Loess Plateau, Northern China, have displayed the coexistence of 100-, 41- and 23-ka periods, with a distinguished 100 kyr periodicity associated with the glacial-interglacial cycle (Beck et al., 2018; Nie et al., 2017; Sun et al., 2015). The local seawater $\delta^{18}O$ of the East China Sea has been dominated by eccentricity and obliquity cycles with almost no precession variance (Clemens et al., 2018). These results suggest that the EASM is affected by more sensitive to high-latitude ice volume variations than to direct insolation changes. In contrast, speleothem $\delta^{18}O$ records from caves in southern China showed an almost pure precession cycle, implying the dominance of direct insolation forcing in summer precipitation over southern China (Cheng et al., 2016; Wang et al., 2008; Zhang et al., 2019). Similarly, a long pollen record from Lake Biwa in Japan contains distinct precession and obliquity signals, suggesting that the EASM has been mainly controlled by insolation forcing, and the effect of ice volume changes becomes predominant only when insolation is weak (Nakagawa et al., 2008).

The different responses of these proxies are probably interpreted as regional heterogeneity in the relative impact of EASM driving forces. For instance, G. Liu et al. (2020) suggested that the lack of glacial-interglacial cycles in the speleothem $\delta^{18}O$ may be explained by the moisture transport pathway effect, in which glacial-interglacial cycles in the monsoon moisture source decrease landward. However, because proxy data are scattered in limited areas, making a spatially continuous interpretation has been difficult. In addition, proxies potentially have complex sensitivity to several climatic factors (e.g., temperature changes and moisture sources), causing difficulty in the interpretation of records (An et al., 2015; Clemens et al., 2010, 2018; X. Liu et al., 2020).

https://doi.org/10.5194/egusphere-2024-307
Preprint. Discussion started: 7 February 2024

To reveal the mechanisms of EASM variability, numerous modelling studies with different boundary conditions have been conducted over the last decades (e.g., Braconnot et al., 2007a; Chen et al., 2011; Dai et al., 2021; Kutzbach, 1981; Kutzbach et al., 2008; Li et al., 2013; Liu et al., 2014; Lyu et al., 2021; Shi et al., 2011; Suarez and Held, 1976; Sun et al., 2015, 2019; Thomas et al., 2016; Weber and Tuenter, 2011; Yin et al., 2008, 2009, 2014; Yin and Berger, 2012; Zhao et al., 2020). Among these, numerous studies have consistently indicated the presence of the 20 kyr precession cycle in summer precipitation in most of the EASM regions（Li et al., 2013; Sun et al., 2015; Lyu et al., 2021; Weber and Tuenter, 2011), suggesting that insolation appears to be the key factor determining the variability of EASM (Dai et al., 2021; Li et al., 2013). The impact of ice volume on summer precipitation varies between regions (Sun et al., 2015; Lyu et al., 2021); for instance, Lyu et al. (2021) indicated that the effect of the glacial-interglacial 100 kyr cycle becomes significant in the 20–25°N region, whereas in other regions, summer precipitation is primarily influenced by the 20 kyr precession cycle. The results suggest that, in the EASM regions, summer rainfall variability is affected by orbital and glacial forcings; however, the relative impact of each forcing differs with the region (e.g., Dai et al., 2021; Sun et al., 2015). The proposed mechanisms that cause the special and temporal variability of the EASM are often attributed to the anomalous western North Pacific subtropical high (sub-high) (Dai et al., 2021; Liu et al., 2014; Sun et al., 2015), which causes shifts in the seasonal Meiyu/Baiu rain bands (Yihui and Chan, 2005) and variation in southerly wind provides moisture into EASM regions (Liu et al., 2014). However, the simulated regionalities varied between studies owing to the unclear position of the sub-high depending on models (Dai et al., 2021), and the detailed mechanisms of the sub-high fluctuation remain ambiguous. In addition, determining the individual impact of insolation and ice volume changes on EASM variability remains challenging because of the complex relationship between orbital and glacial forcings (Yin et al., 2014; Lyu et al., 2021). Thus, monsoon variability under individual forcing (insolation or ice volume) should be analysed more substantially in terms of the global climate system, including atmospheric circulation, atmosphere-ocean interactions, and teleconnections.

In the present study, we aimed to reassess the relative impact of insolation changes on EASM variability. We conducted 450 kyr-long idealised, time-sliced simulations with a boundary condition of the Earth's three orbital parameters (Berger and Loutre, 1999) to reconstruct orbital-scale EASM variability using a global climate model. Using the time slice method, the quasi-equilibrium climate state of each period was calculated at an interval of 5 kyr. This study reveals the possible mechanisms resulting in regionally differing responses of EASM variability to insolation changes through data-model comparisons over East Asia. Section 2 describes the climate model and the experimental design (or datasets). Section 3 explains the model results and compares the numerical results with proxy data. Section 4 discusses the possible climate systems that drive EASM variability, which causes the known regionality of proxy data. In Section 5, we summarise and conclude the paper.

https://doi.org/10.5194/egusphere-2024-307
Preprint. Discussion started: 7 February 2024

2 Model and experimental design

2.1 Model

Experiments were performed using the Meteorological Research Institute Coupled General Circulation Model version 2.3 (MRI-CGCM2.3) (Yukimoto et al., 2006). This model comprises an atmospheric general circulation model (AGCM) and a global ocean general circulation model (OGCM). The atmospheric component of the model was a spectral model with T42 spatial resolution (approximately 2.8°) and 30 vertical layers, which was based on Shibata et al. (1999). The oceanic component of the model was a Bryan–Cox-type ocean general circulation model with a horizontal resolution of 2.5° longitude and 2.0–0.5° latitude and 23 vertical layers. Details of the model are described in Yukimoto et al. (2006).

MRI-CGCM has been widely used for future climate prediction (e.g., Kitoh, 2007; Ueda et al., 2006) and paleoclimate simulations (e.g., Braconnot et al., 2007a; Kamae et al., 2016, 2017; Kitoh et al., 2007; Ueda et al., 2011). The reproducibility of MRI-CGCM2.3 has already been studied by Yukimoto et al. (2006) and indicates good agreement with observations in the distribution of surface air temperature and precipitation. The model effectively simulates summer precipitation over East Asia, including their onset timing and migration (Yukimoto et al., 2006), and has been used for paleo-Asian monsoon simulations, including the Last Glacial Maximum (LGM) (Ueda et al., 2011), the Medieval Warm Period, and Little Ice Age (Kamae et al., 2017).

2.2 Experimental design

We used a time-slice approach by dividing the last 450 kyr into 91 periods (5 kyr intervals). The quasi-equilibrium climate state was evaluated during each period. While this approach may not fully capture the transient behaviour of climate systems, as demonstrated in recent transient simulations (Chen et al., 2011; Clemens et al., 2018; Kutzbach et al., 2008; Timmermann et al., 2007), the mean climate states obtained through the time-slice method are well-suited for evaluating the responses of prescribed external forcings to monsoon variability. This methodology has been employed in numerous studies (Kutzbach, 1981; Liu et al., 2014; Wen et al., 2016). The time slice approach adopted can calculate the long-term integral in the same period, enabling us to discuss the seasonal evolution of the EASM in addition to long-term climate responses to orbital forcing (Cubasch et al., 1995).

As a boundary condition, insolation was calculated from the Earth's three orbital parameters (longitude of perihelion as precession, obliquity, and eccentricity) at each corresponding time period based on Berger and Loutre (1999). In all the time-sliced experiments, any other time-varying boundary conditions, such as vegetation, the concentration of greenhouse gases, ice sheets, topography, and land-sea boundaries, were prescribed at the pre-industrial (PI; 0 ka) level. In particular, the concentration of greenhouse gases was set to the same value as that of the Paleo-climate Modelling Intercomparison Project 2 (PMIP2) (Braconnot et al., 2007a, 2007b). Although ice volume changes and variations in greenhouse gas concentrations might have a potential effect on EASM variability (Clemens et al., 2018; Yin et al., 2008; Yin and Berger, 2012), we only focused on the effect of orbital changes to evaluate the relative impact of insolation changes on EASM. All experiments were

https://doi.org/10.5194/egusphere-2024-307
Preprint. Discussion started: 7 February 2024

conducted without any flux adjustments. To eliminate the effects of climate drift (Kitoh et al., 2007), the model was integrated for 230 years prior to the main experiments. Then, the result of the 230th year was forwarded to the main experiments as an initial condition. After integrating another 55 years into the main experiments, the average output of the last 50 years was analysed as the representative climate state of each time period.

3 Results

In the present study, 'anomaly' was defined as the difference in climate state between PI and each time period. In addition, we defined a strong period (SP) as the period in which the summer insolation anomaly at the top of the atmosphere in low-mid latitude (20° N–40° N) was over 1 standard deviation. Seasonality was discussed based on the Northern Hemisphere seasons. Specifically, this section used 'summer' to refer to June–August (JJA). Unless otherwise noted, all the correlation coefficients calculated in this study exceeded the 99.9 % confidence level using Pearson's t-test.

3.1 Model reconstructed precipitation variability

In this section, we describe the calculation results of summer precipitation variability and its predominant cycles in the three main EASM regions (South East China: SEC, Chinese Loess Plateau: CLP, Japan: JP), defined as follows: SEC (24° N–33° N, 105° E–120° E), CLP (34° N–38° N, 100° E–110° E), and JP (30° N–40° N, 130° E–143° E) (Fig. 1). Figure 2 shows the calculated temporal variation in summer precipitation over the last 450 kyr. Summer precipitation variability in SEC and CLP had a strong similarity to summer insolation change, and the maxima of summer precipitation precisely coincided with the SPs of summer insolation (Fig. 2a; hatched area). Furthermore, we found a strong positive correlation between summer insolation and precipitation over SEC ($R = 0.94, p < 0.001$) and CLP ($R = 0.78, p < 0.001$) (Fig. 3). The results confirm the significance of the insolation effect on the variability of EASM in China, as suggested by previous calculations using different models, such as CCSM3 (Li et al., 2013) and HadCM3 (Lyu et al., 2021). In JP, the relationship between summer insolation and precipitation was relatively unclear; however, the minima of summer precipitation corresponded to some summer insolation SPs (Fig. 2a). The correlation coefficient between summer insolation and precipitation in JP showed a negative correlation ($R = -0.63, p < 0.001$), although it was unclear when compared to SEC and CLP (Fig. 3). These results suggest that the effect of summer insolation on precipitation varies between regions, with notable differences in the response observed between China and Japan.

The periodicity of change in summer precipitation in each region had different characteristics (Fig. 2b). In the SEC and CLP, summer precipitation was dominated by precession bands (19 and 23 kyr), whereas in JP, it was dominated by an obliquity band (41 kyr), and the precession bands were not as strong as in SEC and CLP. A slight 56 kyr band was found in the CLP summer precipitation variability, which was neither visible in insolation nor in other regions. A 100 kyr eccentricity band was not found in any region because the effect of eccentricity on insolation is generally minimal compared to that of precession and obliquity (Schneider et al., 2011).

https://doi.org/10.5194/egusphere-2024-307
Preprint. Discussion started: 7 February 2024

3.2 Comparison with proxies

We compared the model results with proxy data in Fig. 2: the oxygen isotope ratio records ($\delta^{18}O$) of speleothems from Chinese caves (located in SEC) (Cheng et al., 2016), meteoric ^{10}Be preserved in Pleistocene Chinese loess (CLP) (Beck et al., 2018), and a pollen record from Lake Biwa (JP) (Nakagawa et al., 2008). The represented monsoon index differed between proxies. Speleothem $\delta^{18}O$ is used to document summer monsoon variability (Wang et al., 2017), whereas CLP ^{10}Be records indicate the annual amount of precipitation, which can be treated as summer precipitation according to Beck et al. (2018). The pollen record in JP represents amounts from April to September (Nakagawa et al., 2008).

The model results were highly consistent with the cave $\delta^{18}O$ records in the SEC (Fig. 2a): correlation between calculated summer precipitation and $\delta^{18}O$ records in the SEC was $R = -0.56$ $(p < 0.001)$. The power spectrum densities also exhibited good agreement between the model results and proxy data; only the precession cycle was distinguished in the SEC (Fig. 2b). Proxy records from Chinese caves may be affected by climatic factors beyond summer precipitation variability (e.g., Clemens et al., 2010; Wang et al., 2017). For instance, Clemens et al. (2010) proposed that the speleothem $\delta^{18}O$ may reflect winter temperature variability. Nevertheless, our calculation results indicate that changes in solar insolation alone have an impact on summer precipitation in China. The calculated variation in summer rainfall in the CLP was consistent with that of proxy data (Fig. 2a), although the correlation was not as strong as in the SEC ($R = 0.42, p < 0.001$). The eccentricity band was dominant in the proxy data, whereas the precession band was the strongest signal in the model results (Fig. 2b). The slight 56 kyr signal in the model results was also found in proxy data (Fig. 2b). These characteristics support the idea that summer precipitation variability in China is strongly influenced by changes in summer insolation, particularly in SEC. The inconsistency between proxy and model results in CLP indicates that, although insolation certainly affects summer precipitation variability in Northern China, the actual variability of summer precipitation should also be influenced by other forcings not considered in this study, such as global ice volume change and variation in greenhouse gases.

The calculated summer rainfall variability in JP appeared to be inconsistent with the rainfall reconstructed from proxy data (Fig. 2a), with the correlation being negative and below a significant level ($R = -0.23$ $p = 0.01$). The similarity in the dominant cycles (dominance of precession and obliquity bands) between the model results and proxy data may support the idea that changes in summer insolation affect the monsoon variability in JP (Fig. 2b). However, inconsistency between the model results and proxy data indicates that the summer rainfall in JP represented by pollen records cannot be fully interpreted by the insolation effect; it contains the effect of complex climatic forcings.

4 Discussion

4.1 Mechanism of in-phase variability in South East China and Chinese Loess Plateau

Figure 4 depicts the composite distribution of summer precipitation anomalies in the SPs, along with anomalies in sea level pressure (SLP) and winds. The increase in precipitation was observed over China, and the trend was more pronounced in the SEC (Fig. 4). Similar spatial heterogeneity has been reported in Sun et al. (2015), where insolation forcing had a more

https://doi.org/10.5194/egusphere-2024-307
Preprint. Discussion started: 7 February 2024

significant impact on low-latitude and coastal areas in China. It has been suggested that sub-high variability played an important role in past monsoon variability over East Asia (Dai et al., 2021; Liu et al., 2014; Sun et al., 2015). Correspondingly, the anomalously high pressure was noticeable in our results over the Philippine seas, which intensifies southerly winds at their western edge (Fig. 4). Therefore, we suggest that, under intense solar insolation, the active moisture transport resulting from the strengthened southerly wind at the western edge of the sub-high led to increased summer precipitation over China. This effect would be more significant in SEC than in CLP. The actual summer precipitation in CLP should further decrease during the glacial periods (Sun et al., 2015), as the global cooling and a reduced land-ocean pressure gradient contrast weaken the EASM circulation (Lyu et al., 2021).

Figure 5 depicts the distribution of the sea surface temperature (SST) and surface wind anomalies in SPs. SST increased over almost the entire Indian Ocean except for the central equational region (Fig. 5), corresponding to increasing summer precipitation over the Indian Ocean (Fig. 4). In the modern climate, the sub-high is considered to be formed and maintained through air-sea interaction over the Indo and western Pacific Ocean (Xie et al., 2016). The warming of the Indian Ocean excites the Matsuno–Gill response (Gill, 1980; Matsuno, 1966) through tropospheric Kelvin wave propagation, forcing the anomalous anticyclone over the South China Sea in summer (Xie et al., 2009). The notable consistency of basin-wide warming of the Indian Ocean and extended easterly winds to the western Pacific indicates that the same mechanisms can be applied to increasing EASM rainfall in SP. The tropospheric Kelvin wave propagation frequently occurs in SPs. Although the enhanced sub-high appears to be inconsistent with the warming South China Sea regarding local air-sea feedback (Fig. 5), it may be explained that the effect of the Indian Ocean overwhelms the local SST feedback (Xie et al., 2009).

Xie et al. (2016) demonstrated that wind–evaporation–SST (WES) feedback also contributes to the formation and maintenance of the sub-high in spring. According to Wang et al. (2000), the WES feedback is as follows: SST cooling over the western North Pacific suppresses in situ convective heating, exciting a westward-propagating Rossby wave. The intensified northeast trades at the eastern edge of the anomalous anticyclone amplified the initial SST cooling via evaporation and wind stirring. To investigate whether WES feedback also occurred in the past, we verified the distribution of SST anomalies in spring (MAM) in the SPs. The SST cooling band extending from southwest to northeast and the in situ anomalous high were identified over the western North Pacific (Fig. 6). Furthermore, the anomalous high was slightly west of the negative SST region, suggesting that northerly winds intensified mean northeast trades (Fig. 6). Thus, the WES feedback may have formed and maintained the sub-high in spring when summer insolation was strong, increasing the monsoon rainfall over the SEC and CLP. Though the increase in SEC and CLP was attributed to the changes in SST, the causal mechanisms connecting solar insolation changes and SST anomalies remained unclear in this study, which would be an important future study.

4.2 Mechanism of anti-phase variability in Japan

The inverse phase between summer insolation and precipitation around JP was found in the model results (Fig. 3). Composite SLP anomalies over the North Pacific region (Fig. 4) indicate that the salient anomalous North Pacific High (NPH), with a maximum at approximately 35° N 170° E was pronounced (~5 hPa) in SPs, the western edge of which overlaps around

https://doi.org/10.5194/egusphere-2024-307
Preprint. Discussion started: 7 February 2024

JP and reduces summer rainfall (Fig. 4). In modern climatology, the variation in NPH is often attributed to the thermal contrast of diabatic heating between land and sea (Rodwell and Hoskins, 2001; Miyasaka and Nakamura, 2005). For example, the intensified thermal contrast between the North Pacific Ocean and North American continent results in a stronger northerly wind over the western coast of the North American continent and cools SST by the enhanced coastal upwelling. As a result, the NPH may be intensified due to the parasol effect and/or radiative cooling because low-level clouds increase when the SST declines (Miyasaka and Nakamura, 2005). In the present study, the anomaly of vertically integrated diabatic heating in SPs was positive over the North American continent and negative over the North Pacific Ocean (Fig. 7a). Notably, the large sensible heating was found over land, contributing to the warming of the North American continent (Fig. 7b). In contrast, a negative anomaly in latent heat was observed over North Pacific Ocean (Fig. 7c). These features indicate the enhancement of thermal contrast in SPs, consistent with the intensification of NPH. The tropics, including the Maritime Continent, were characterised by remarkable diabatic heating anomalies (Fig. 7a). The anomaly derived mainly from latent heat (Fig. 7c), suggesting less convective activity over the South China and Philippine seas. The climate system discussed here may not reflect the actual variability because the model results did not reproduce the temporal variation suggested by proxies. Thus, the impact of additional forcing (ice sheets and greenhouse gases) on the precipitation in JP should be analysed in future studies.

5 Conclusions

The present study aimed to quantitatively assess the effects of insolation changes based on the three orbital parameters on EASM variability. The results showed that the increase in Northern Hemisphere insolation strongly intensifies the summer precipitation over China. This can be attributed to a climate system similar to the IPOC mode known in modern climatology. From spring to early summer in SPs, the WES feedback via negative SST anomalies in the tropical western North Pacific and the warming of the Indian Ocean in summer sustains the western Pacific subtropical high. The western Pacific subtropical high enhances the water vapour transport to the north, subsequently increasing the EASM rainfall in the SEC and CLP. In contrast, the model results showed that the increase in insolation causes the suppression of the summer precipitation in JP through the intensification of NPH. The model results coincide with the proxy records in the SEC region, whereas they were apparently inconsistent with proxy records in CLP and JP. This implies that insolation changes must have controlled the EASM rainfall in the SEC, but other external forcings, such as changes in ice volume and greenhouse gases, markedly influence the EASM variability in CLP and JP. Numerical experiments considering further external forcings, such as ice sheet volume and greenhouse gas fluctuations, are expected to clarify the actual EASM variability and its complex intrinsic system.

Author contribution

TM, MH, HU, and TN designed this study. TM performed experiments. TM and MH wrote the manuscript. All the authors discussed the results and commented on the manuscript.

https://doi.org/10.5194/egusphere-2024-307
Preprint. Discussion started: 7 February 2024

Code/Data availability

The data that support the findings of this study are available from the corresponding author, upon reasonable request.

Competing interests

The authors declare that they have no conflict of interest.

Acknowledgements

This work was supported by JSPS KAKENHI Grant Number 21H01197.

References

An, Z., Wu, G., Li, J., Sun, Y., Liu, Y., Zhou, W., Cai, Y., Duan, A., Li, L., Mao, J., Cheng, H., Shi, Z., Tan, L., Yan, H., Ao, H., Chang, H., and Feng, J.: Global monsoon dynamics and climate change. Annu. Rev. Earth Planet. Sci., 43, 29–77, https://doi.org/10.1146/annurev-earth-060313-054623, 2015.

Abe-Ouchi, A., Saito, F., Kawamura, K., Raymo, M. E., Okuno, J., Takahashi, K., and Blatter, H.: Insolation-driven 100,000-year glacial cycles and hysteresis of ice-sheet volume, Nature, 500, 190–193, https://doi.org/10.1038/nature12374, 2013.

Beck, J. W., Zhou, W., Li, C., Wu, Z., White, L., Xian, F., Kong, X., and An, Z.: A 550,000-year record of East Asian monsoon rainfall from ^{10}Be in loess, Science, 360, 877–881, https://doi.org/10.1126/science.aam5825, 2018.

Berger, A. L.: Long-term variations of daily insolation and Quaternary climatic changes, J. Atmos. Sci., 35, 2362–2367, https://doi.org/10.1175/1520-0469(1978)035<2362:LTVODI>2.0.CO;2, 1978.

Berger, A. L. and Loutre, M.-F.: Parameters of the Earths orbit for the last 5 million years in 1 kyr resolution, Pangea, https://doi.org/10.1594/PANGAEA.56040, 1999.

Berger, A. and Loutre, M. F.: Insolation values for the climate of the last 10 million years, Quat. Sci. Rev., 10, 297–317, https://doi.org/10.1016/0277-3791(91)90033-Q, 1991.

Berger, A., Driesschaert, E., Goosse, H., Loutre, M. F., Crucifix, M.: The Eurasian ice sheet reinforces the East Asian summer monsoon during the interglacial 500 000 years ago, Clim. Past, 4, 79–90, https://doi.org/10.5194/cp-4-79-2008, 2008.

Braconnot, P., Otto-Bliesner, B., Harrison, S., Joussaume, S., Peterchmitt, J. -Y., Abe-Ouchi, A., Crucifix, M., Driesschaert, E., Fichefet, T., Hewitt, C. D., Kageyama, M., Kitoh, A., Laîné, A., Loutre, M. -F., Marti, O., Merkel, U., Ramstein, G., Valdes, P., Weber, S. L., Yu, Y., and Zhao, Y.: Results of PMIP2 coupled simulations of the Mid-Holocene and Last Glacial Maximum - Part 1: Experiments and large-scale features, Clim. Past, 3, 261–277, https://doi.org/10.5194/cp-3-261-2007, 2007a.

Braconnot, P., Otto-Bliesner, B., Harrison, S., Joussaume, S., Peterchmitt, J. -Y., Abe-Ouchi, A., Crucifix, M., Driesschaert, E., Fichefet, T., Hewitt, C. D., Kageyama, M., Kitoh, A., Loutre, M. -F., Marti, O., Merkel, U., Ramstein, G., Valdes,

https://doi.org/10.5194/egusphere-2024-307
Preprint. Discussion started: 7 February 2024

P., Weber, L., Yu, Y., and Zhao, Y.: Results of PMIP2 coupled simulations of the Mid-Holocene and Last Glacial Maximum - Part 2: Feedbacks with emphasis on the location of the ITCZ and mid- and high latitudes heat budget, Clim. Past, 3, 279–296, https://doi.org/10.5194/CP-3-279-2007, 2007b.

Chen, G.-S., Liu, Z., Clemens, S. C., Prell, W. L., and Liu, X.: Modeling the time-dependent response of the Asian summer monsoon to obliquity forcing in a coupled GCM: A PHASEMAP sensitivity experiment, Clim. Dyn., 36, 695–710, https://doi.org/10.1007/s00382-010-0740-3, 2011.

Cheng, H., Edwards, R. L., Sinha, A., Spötl, C., Yi, L., Chen, S., Kelly, M., Kathayat, G., Wang, X., Li, X., Kong, X., Wang, Y., Ning, Y., and Zhang, H.: The Asian monsoon over the past 640,000 years and ice age terminations, Nature, 534, 640–646, https://doi.org/10.1038/nature18591, 2016.

Clemens, S. C., Holbourn, A., Kubota, Y., Lee, K. E., Liu, Z., Chen, G., Nelson, A., and Fox-Kemper, B.: Precession-band variance missing from East Asian monsoon runoff, Nat. Commun., 9, 3364, https://doi.org/10.1038/s41467-018-05814-0, 2018.

Clemens, S. C., Prell, W. L., and Sun, Y.: Orbital-scale timing and mechanisms driving Late Pleistocene Indo-Asian summer monsoons: Reinterpreting cave speleothem $\delta^{18}O$, Paleoceanography and Paleoclimatology, 25, PA4207, https://doi.org/10.1029/2010PA001926, 2010.

Cubasch, U., Waszkewitz, J., Hegerl, G., and Perlwitz, J.: Regional climate changes as simulated in time-slice experiments, Clim. Change, 31, 273–304, https://doi.org/10.1007/BF01095150, 1995.

Dai, G., Zhang, Z., Otterå, O. H., Langebroek, P. M., Yan, Q., and Zhang, R.: A Modeling Study of the Tripole Pattern of East China Precipitation over the Past 425 ka, Geophys. Res. Atmos., 126, e2020, https://doi.org/10.1029/2020JD033513, 2021.

Enomoto, T., Hoskins, B. J., and Matsuda, Y.: The formation mechanism of the Bonin high in August, Q. J. R. Meteorol. Soc., 129, 157–178, https://doi.org/10.1256/qj.01.211, 2003.

Gill, A. E.: Some simple solutions for heat-induced tropical circulation, Q. J. R. Meteorol. Soc., 106, 447–462, https://doi.org/10.1002/qj.49710644905, 1980.

Goldsmith, Y., Broecker, W. S., Xu, H., Polissar, P. J., DeMenocal, P. B., Porat, N., Lan, J., Cheng, P., Zhou, W., and An, Z.: Northward extent of East Asian monsoon covaries with intensity on orbital and millennial timescales, Proc. Natl Acad. Sci. U. S. A., 114, 1817–1821, https://doi.org/10.1073/PNAS.1616708114, 2017.

Kamae, Y., Kawana, T., Oshiro, M., and Ueda, H.: Seasonal modulation of the Asian summer monsoon between the Medieval Warm Period and Little Ice Age: A multi model study, Prog. Earth Planet. Sci., 4, 22, https://doi.org/10.1186/s40645-017-0136-7, 2017.

Kamae, Y., Yoshida, K., and Ueda, H.: Sensitivity of Pliocene climate simulations in MRI-CGCM2.3 to respective boundary conditions, Clim. Past, 12, 1619–1634, https://doi.org/10.5194/cp-12-1619-2016, 2016.

Kitoh, A.: Climate-change simulations: Future climate projections and paleoclimate modeling, Low Temp, Sci., 65, 77–85, http://hdl.handle.net/2115/20457, 2007.

https://doi.org/10.5194/egusphere-2024-307
Preprint. Discussion started: 7 February 2024

Kitoh, A., Motoi, T., and Murakami, S.: El Niño-southern oscillation simulation at 6000 years before present with the MRI-CGCM2.3: Effect of flux adjustment, J. Clim., 20, 2484–2499, https://doi.org/10.1175/JCLI4141.1, 2007.

Kutzbach, J. E.: Monsoon climate of the Early Holocene: Climate experiment with the earth's orbital parameters for 9000 years ago, Science, 214, 59–61, https://doi.org/10.1126/science.214.4516.59, 1981.

Kutzbach, J. E., Liu, X., Liu, Z., and Chen, G.: Simulation of the evolutionary response of global summer monsoons to orbital forcing over the past 280,000 years, Clim. Dyn., 30, 567–579, https://doi.org/10.1007/s00382-007-0308-z, 2008.

Li, X., Liu, X., Qiu, L., An, Z., and Yin, Z.: Transient simulation of orbital-scale precipitation variation in monsoonal East Asia and arid central Asia during the last 150 ka, J. Geophys. Res., 118, 7481–7488. https://doi.org/10.1002/jgrd.50611, 2013.

Lisiecki, L. E. and Raymo, M. E.: A Pliocene-Pleistocene stack of 57 globally distributed benthic $\delta^{18}O$ records, Paleoceanography and Paleoclimatology, 20, https://doi.org/10.1029/2004PA001071, 2005.

Liu, G., Li, X., Chiang, H. W., Cheng, H., Yuan, S., Chawchai, S., He, S., Lu, Y., Aung, L. T., Maung, P. M., Tun, W. N., Oo, K. M., and Wang, X.: On the glacial-interglacial variability of the Asian monsoon in speleothem $\delta^{18}O$ records, Sci. Adv., 6, eaay8189, https://doi.org/10.1126/sciadv.aay8189, 2020.

Liu, X., Liu, J., Chen, S., Chen, J., Zhang, X., Yan, J., and Chen, F.: New insights on Chinese cave $\delta^{18}O$ records and their paleoclimatic significance, Earth Sci. Rev., 207, 103216, https://doi.org/10.1016/j.earscirev.2020.103216, 2020.

Liu, Z., Wen, X., Brady, E. C., Otto-Bliesner, B., Yu, G., Lu, H., Cheng, H., Wang, Y., Zheng, W., Ding, Y., Edwards, R. L., Cheng, J., Liu, W., and Yang, H.: Chinese cave records and the east asia summer monsoon, Quat. Sci. Rev., 83, 115–128, https://doi.org/10.1016/j.quascirev.2013.10.021, 2014.

Lyu, A., Yin, Q., Crucifix, M., & Sun, Y.: Diverse regional sensitivity of summer precipitation in East Asia to ice volume, CO_2 and astronomical forcing. Geophys. Res., 48, e2020GL092005. https://doi.org/10.1029/2020GL092005, 2021.

Matsuno, T.: Quasi-geostrophic motions in the equatorial area, J. Meteorol. Soc. Jpn, 44, 25–43, https://doi.org/10.2151/jmsj1965.44.1_25, 1966.

Miyasaka, T., and Nakamura, H.: Structure and formation mechanisms of the northern hemisphere summertime subtropical highs. J. Clim., 18, 5046–5065, https://doi.org/10.1175/JCLI3599.1, 2005.

Nakagawa, T., Okuda, M., Yonenobu, H., Miyoshi, N., Fujiki, T., Gotanda, K., Tarasov, P. E., Morita, Y., Takemura, K., and Horie, S.: Regulation of the monsoon climate by two different orbital rhythms and forcing mechanisms, Geol., 36, 491–494, https://doi.org/10.1130/G24586A.1, 2008.

Nie, J., Garzione, C., Su, Q., Liu, Q., Zhang, R., Heslop, D., Necula, C., Zhang, S., Song, Y., and Luo, Z.: Dominant 100,000-year precipitation cyclicity in a Late Miocene lake from northeast Tibet, Sci. Adv., 3, e1600762, https://doi.org/10.1126/sciadv.1600762, 2017.

Rodwell, M. J., and Hoskins, B. J.: Subtropical anticyclones and summer monsoons. J. Clim., 14, 3192–3211, https://doi.org/10.1175/1520-0442(2001)014<3192:SAASM>2.0.CO;2, 2001.

Schneider, S. H., Root, T. L., and Mastrandrea, M. D.: Encyclopedia of climate and weather, Oxford University Press, 2011.

https://doi.org/10.5194/egusphere-2024-307
Preprint. Discussion started: 7 February 2024

Shi, Z. G., Liu, X. D., Sun, Y. B., An, Z. S., Liu, Z., and Kutzbach, J.: Distinct responses of East Asian summer and winter monsoons to astronomical forcing, Clim. Past, 7, 1363–1370, https://doi.org/10.5194/CP-7-1363-2011, 2011.

Shibata, K., Yoshimura, H., Ohizumi, M., Hosaka, M., and Sugi, M.: A simulation of troposphere, stratosphere and mesosphere with an MRI/JMA98 GCM, Pap. Meteorol. Geophys., 50, 15–53, https://doi.org/10.2467/mripapers.50.15, 1999.

Suarez, M. J. and Held, I. M.: Modelling climatic response to orbital parameter variations, Nature, 263, 46–47, https://doi.org/10.1038/263046a0, 1976.

Sun, Y., Chen, J., Clemens, S. C., Liu, Q., Ji, J., and Tada, R.: East Asian monsoon variability over the last seven glacial cycles recorded by a loess sequence from the northwestern Chinese Loess Plateau, Geochem. Geophys. Geosyst., 7, 12, Q12Q02, https://doi.org/10.1029/2006GC001287, 2006.

Sun, Y., Kutzbach, J., An, Z., Clemens, S., Liu, Z., Liu, W., Liu, X., Shi, Z., Zheng, W., Liang, L., Yan, Y., and Li, Y.: Astronomical and glacial forcing of East Asian summer monsoon variability, Quat. Sci. Rev., 115, 132–142, https://doi.org/10.1016/j.quascirev.2015.03.009, 2015.

Sun, Y., Yin, Q., Crucifix, M., Clemens, S. C., Araya-Melo, P., Liu, W., Qiang, X., Liu, Q., Zhao, H., Liang, L., Chen, H., Li, Y., Zhang, L., Dong, G., Li, M., Zhou, W., Berger, A., and An, Z.: Diverse manifestations of the mid-Pleistocene climate transition, Nat. Commun., 10, 352, https://doi.org/10.1038/s41467-018-08257-9, 2019.

Thomas, E. K., Clemens, S. C., Sun, Y., Prell, W. L., Huang, Y., Gao, L., et al.: Heterodynes dominate precipitation isotopes in the East Asian monsoon region, reflecting interaction of multiple climate factors. Earth Planet. Sci. Lett., 455, 196–206. https://doi.org/10.1016/j.epsl.2016.09.044, 2016.

Timmermann, A., Lorenz, S. J., An, S. I., Clement, A., and Xie, S.-P.: The effect of orbital forcing on the mean climate and variability of the tropical Pacific, J. Clim., 20, 4147–4159, https://doi.org/10.1175/JCLI4240.1, 2007.

Ueda, H., Iwai, A., Kuwako, K., and Hori, M. E.: Impact of anthropogenic forcing on the Asian summer monsoon as simulated by eight GCMs, Geophys. Res. Lett., 33, L06703, https://doi.org/10.1029/2005GL025336, 2006.

Ueda, H., Kuroki, H., Ohba, M., and Kamae, Y.: Seasonally asymmetric transition of the Asian monsoon in response to ice age boundary conditions, Clim. Dyn., 37, 2167–2179, https://doi.org/10.1007/s00382-010-0975-z, 2011.

Wang, B., Wu, R., and Fu, X.: Pacific-East Asian teleconnection: How Does ENSO Affect East Asian climate?, J. Clim., 13, 1517–1536, https://doi.org/10.1175/1520-0442(2000)013<1517:PEATHD>2.0.CO;2, 2000.

Wang, P. X., Wang, B., Cheng, H., Fasullo, J., Guo, Z., Kiefer, T., and Liu, Z.: The global monsoon across time scales: Mechanisms and outstanding issues, Earth Sci. Rev., 174, 84–121, https://doi.org/10.1016/j.earscirev.2017.07.006, 2017.

Wang, Y., Cheng, H., Edwards, R. L., Kong, X., Shao, X., Chen, S., Wu, J., Jiang, X., Wang, X., and An, Z.: Millennial- and orbital-scale changes in the East Asian monsoon over the past 224,000 years, Nature, 451, 1090–1093, https://doi.org/10.1038/nature06692, 2008.

Weber, S. L., & Tuenter, E.: The impact of varying ice sheets and greenhouse gases on the intensity and timing of boreal summer monsoons. Quat. Sci. Rev., 30, 469–479. https://doi.org/10.1016/j.quascirev.2010.12.009, 2011.

https://doi.org/10.5194/egusphere-2024-307
Preprint. Discussion started: 7 February 2024

Wen, X., Liu, Z., Wang, S., Cheng, J., and Zhu, J.: Correlation and anti-correlation of the East Asian summer and winter monsoons during the last 21,000 years, Nat. Commun., 7, 11999, https://doi.org/10.1038/ncomms11999, 2016.

Xie, S.-P., Hu, K., Hafner, J., Tokinaga, H., Du, Y., Huang, G., and Sampe, T.: Indian Ocean capacitor effect on Indo-Western pacific climate during the summer following El Niño, J. Clim., 22, 730–747, https://doi.org/10.1175/2008JCLI2544.1, 2009.

Xie, S.-P., Kosaka, Y., Du, Y., Hu, K., Chowdary, J. S., and Huang, G.: Indo-western Pacific Ocean capacitor and coherent climate anomalies in post-ENSO summer: A review, Adv. Atmos. Sci., 33, 411–432, https://doi.org/10.1007/s00376-015-5192-6, 2016.

Yihui, D. and Chan, J. C. L.: The East Asian summer monsoon: An overview, Meteorol. Atmos. Phys., 89, 117–142, https://doi.org/10.1007/s00703-005-0125-z, 2005.

Yin, Q. Z. and Berger, A.: Individual contribution of insolation and CO_2 to the interglacial climates of the past 800,000 years, Clim. Dyn., 38, 709–724, https://doi.org/10.1007/S00382-011-1013-5, 2012.

Yin, Q. Z., Berger, A., and Crucifix, M.: Individual and combined effects of ice sheets and precession on MIS-13 climate, Clim. Past, 5, 229–243, https://doi.org/10.5194/CP-5-229-2009, 2009.

Yin, Q. Z., Singh, U. K., Berger, A., Guo, Z. T., and Crucifix, M.: Relative impact of insolation and the Indo-Pacific warm pool surface temperature on the East Asia summer monsoon during the MIS-13 interglacial, Clim. Past, 10, 1645–1657, https://doi.org/10.5194/CP-10-1645-2014, 2014.

Yukimoto, S., Noda, A., Kitoh, A., Hosaka, M., Yoshimura, H., Uchiyama, T., Shibata, K., Arakawa, O., and Kusunoki, S.: Present-Day Climate and Climate Sensitivity in the Meteorological Research Institute Coupled GCM version 2.3 (MRI-CGCM2.3), J. Meteorol. Soc. Jpn, 84, 333–363, https://doi.org/10.2151/jmsj.84.333, 2006.

Zhang, H., Brahim, Y. A., Li, H., Zhao, J., Kathayat, G., Tian, Y., Baker, J., Wang, J., Zhang, F., Ning, Y., Edwards, R. L., and Cheng, H.: The Asian summer monsoon: Teleconnections and forcing mechanisms—A review from Chinese speleothem $\delta^{18}O$ records, Quaternary, 2, 26, https://doi.org/10.3390/quat2030026, 2019.

Zhao, D., Wan, S., Lu, Z., Zhai, L., Feng, X., Shi, X., and Li, A.: Response of heterogeneous rainfall variability in East Asia to Hadley circulation reorganization during the late Quaternary, Quat. Sci. Rev., 247, 106562, https://doi.org/10.1016/j.quascirev.2020.106562, 2020.

https://doi.org/10.5194/egusphere-2024-307
Preprint. Discussion started: 7 February 2024

Figures

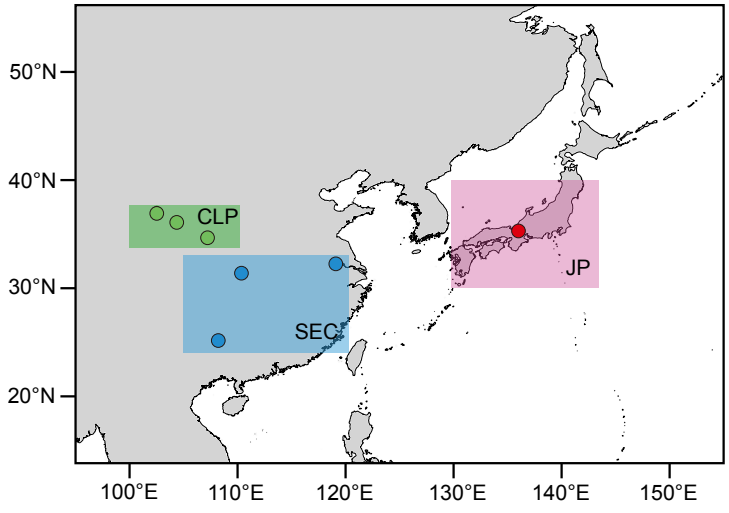

Figure 1. Three EASM regions defined in this study. Blue: South East China (24° N–33° N, 105° E–120° E), green: Chinese Loess Plateau (34° N–38° N, 100° E–110° E), red: Japan (30° N–40° N, 130° E–143° E). Circle plots indicate the locations of proxy records (Beck et al., 2018; Cheng et al., 2016; Nakagawa et al., 2008; Sun et al., 2015). The map was created using the free and open source QGIS.

https://doi.org/10.5194/egusphere-2024-307
Preprint. Discussion started: 7 February 2024

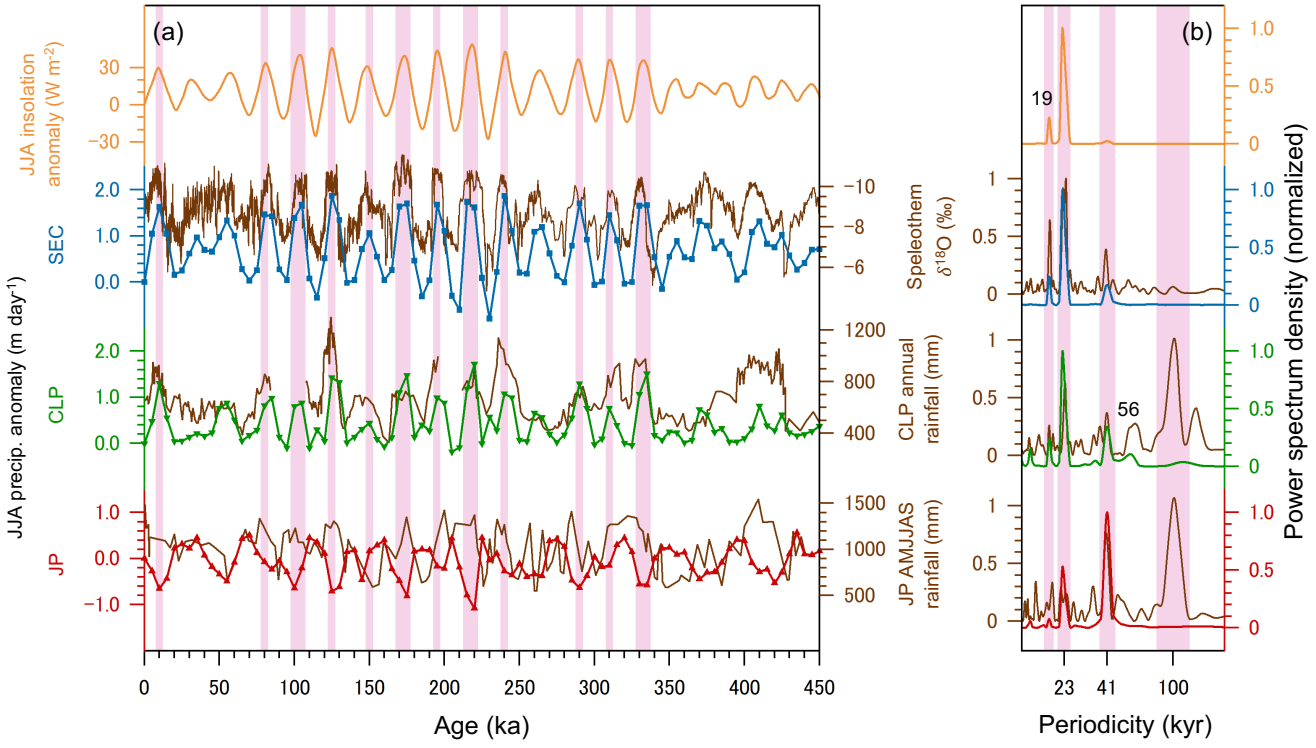

425 **Figure 2.** (a) Temporal variation in calculated JJA insolation anomaly (orange, W m^{-2}), precipitation anomaly in SEC (blue), CLP (green), and JP (red). Insolation was averaged over 20° N–40° N. The precipitation anomaly unit is mm day^{-1}. Brown lines indicate proxy records: Speleothem $\boldsymbol{\delta}^{18}O$ over South East China (‰, Cheng et al., 2016), Be^{10}-based annual rainfall over the Chinese Loess Plateau (mm, Beck et al., 2018), and pollen-based annual temperature variability in Lake Biwa, Japan (K, Nakagawa et al., 2008). Vertical pink bars in (a) denote strong periods (SP). (b) Normalized power spectrum density of (a)
430 (kyr). Vertical pink bars in (b) denote the main orbital cycles (precession, obliquity, and eccentricity).

https://doi.org/10.5194/egusphere-2024-307
Preprint. Discussion started: 7 February 2024

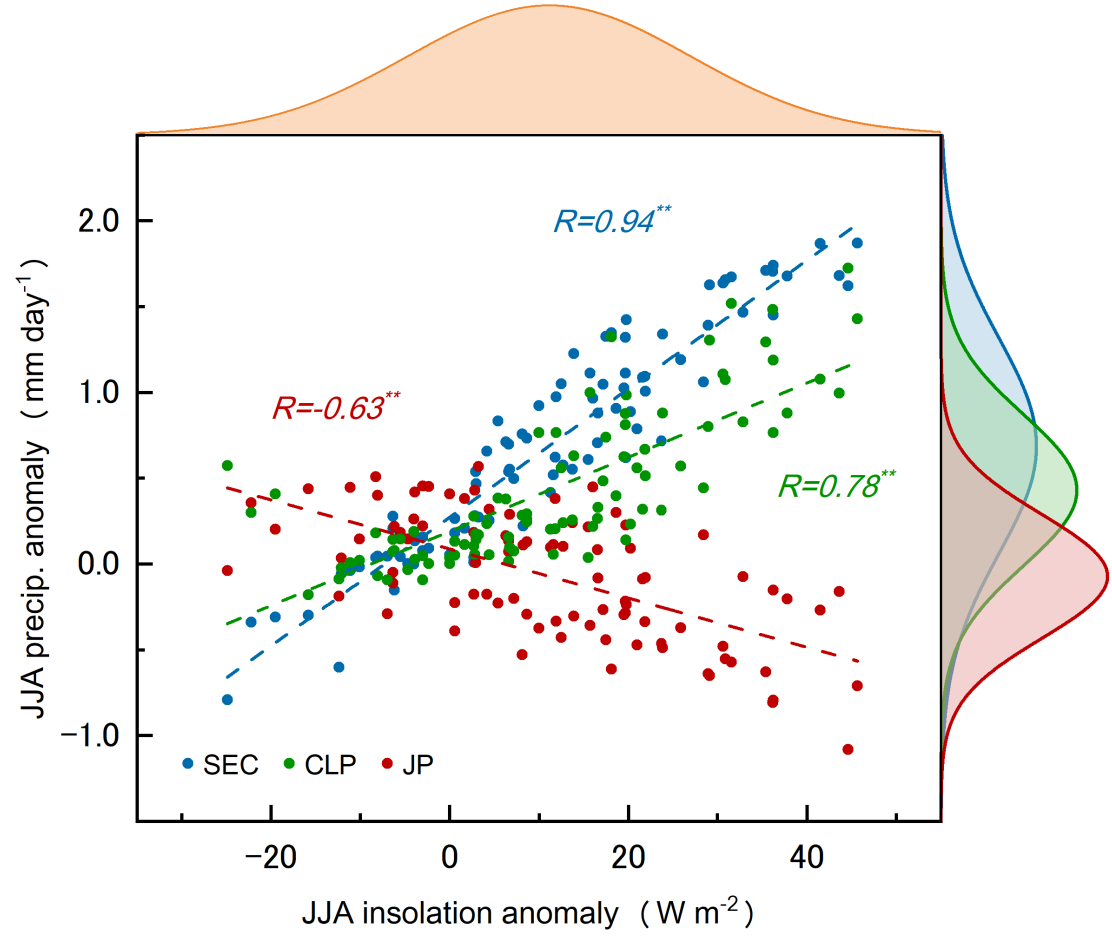

435 **Figure 3.** Correlation between the calculated JJA insolation (W m^{-2}) and precipitation (mm day^{-1}) anomalies of three EASM regions (SEC, CLP, and JP). Insolation was averaged over 20° N–40° N. Figures in the diagram show correlation coefficients.

https://doi.org/10.5194/egusphere-2024-307
Preprint. Discussion started: 7 February 2024

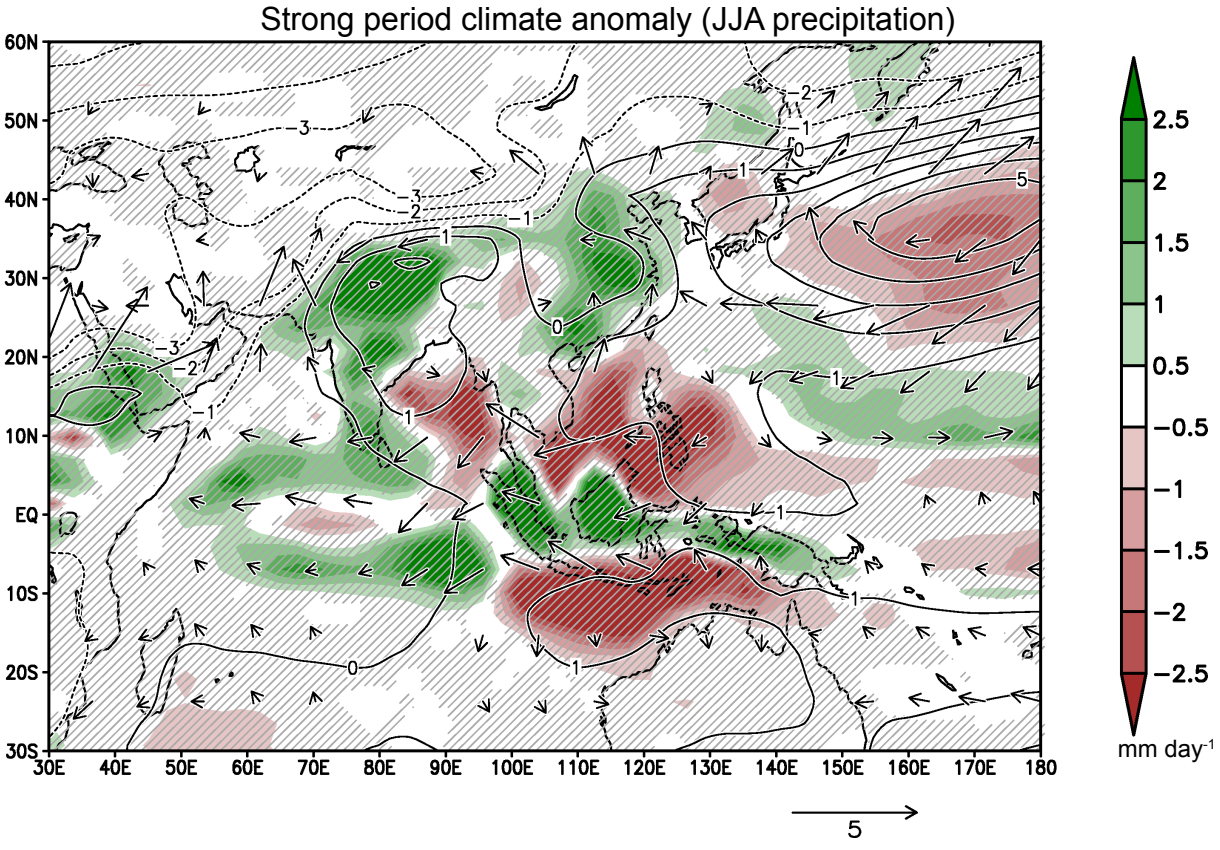

Figure 4. Spatial distribution of the JJA precipitation (shading, mm day^{-1}), sea level pressure (contour, hPa), and surface wind (vector, m s^{-1}) anomalies in strong periods. Solid and dashed lines denote positive and negative, respectively. Surface wind anomaly under 0.1 m s^{-1} is masked. Hatched area denotes regions exceeding a 95 % confidence level using Student's t-test.

https://doi.org/10.5194/egusphere-2024-307
Preprint. Discussion started: 7 February 2024

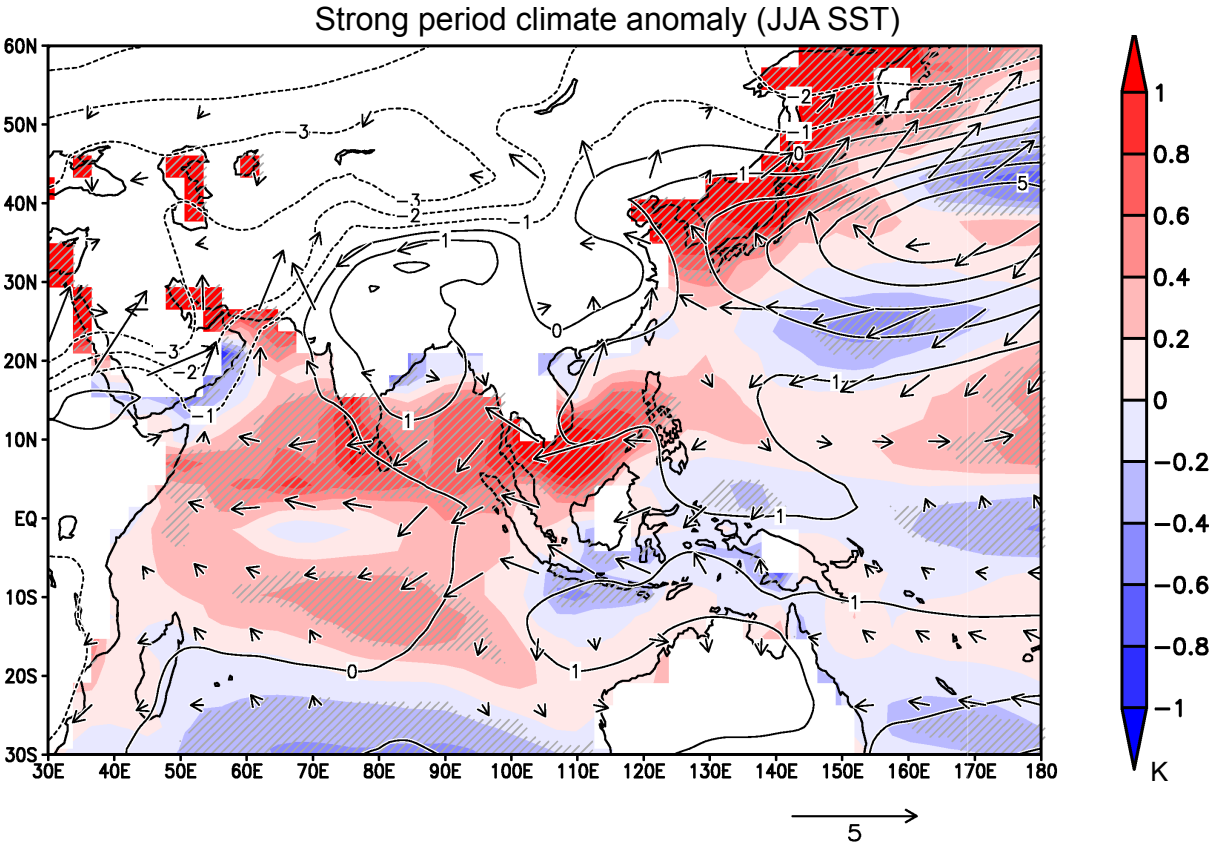

Figure 5. Spatial distribution of the JJA sea surface temperature (shading, K), sea level pressure (contour, hPa), and surface wind (vector, m s^{-1}) anomalies in strong periods. Solid and dashed lines denote positive and negative, respectively. Surface wind anomaly under 0.1 m s^{-1} is masked. Hatched area denotes regions exceeding a 95 % confidence level using Student's t-test.

https://doi.org/10.5194/egusphere-2024-307
Preprint. Discussion started: 7 February 2024

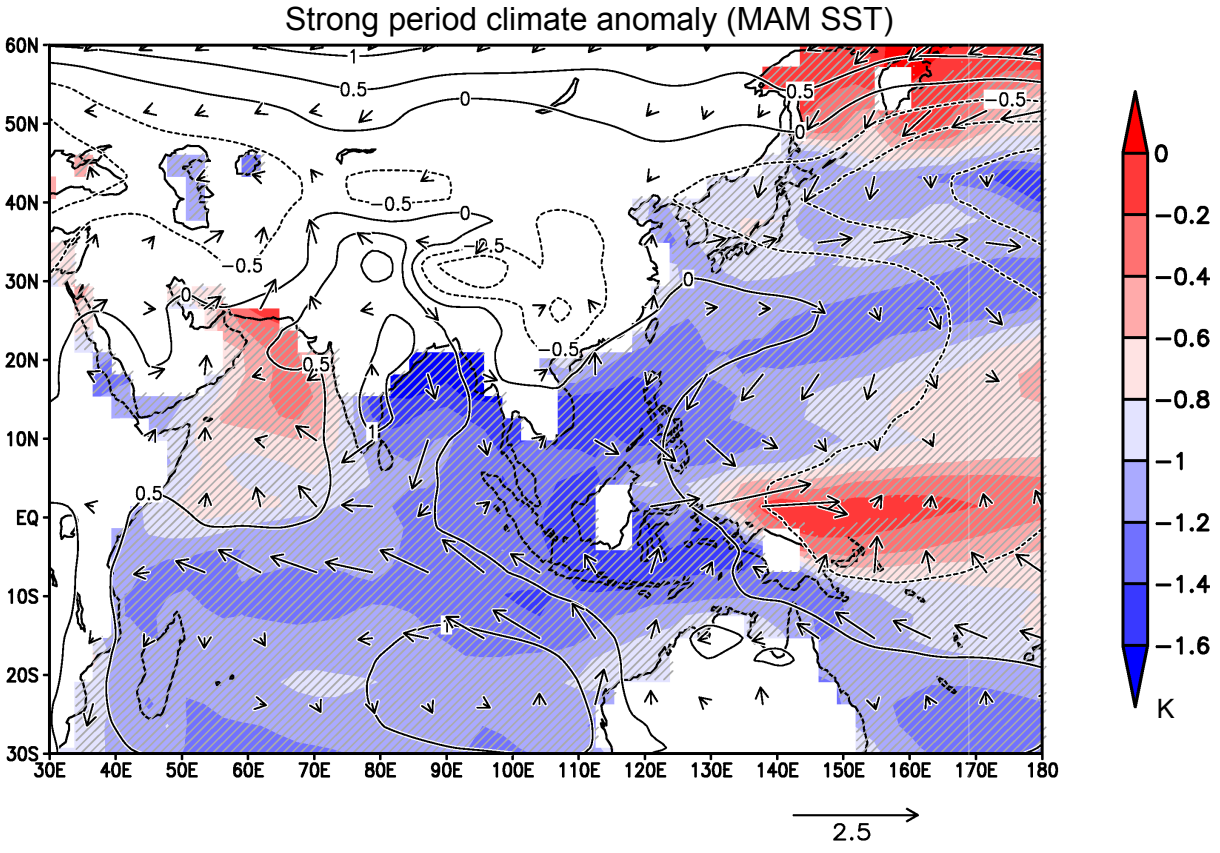

Figure 6. Spatial distribution of spring (MAM) sea surface temperature (shading, K), sea level pressure (contour, hPa), and surface wind (vector, m s^{-1}) anomalies in strong periods. Solid and dashed lines denote positive and negative, respectively. Surface wind anomaly under 0.1 m s^{-1} is masked. Hatched area denotes regions exceeding a 95 % confidence level using Student's t-test. Note that the colour bar in this diagram differs from Fig. 5.

https://doi.org/10.5194/egusphere-2024-307
Preprint. Discussion started: 7 February 2024

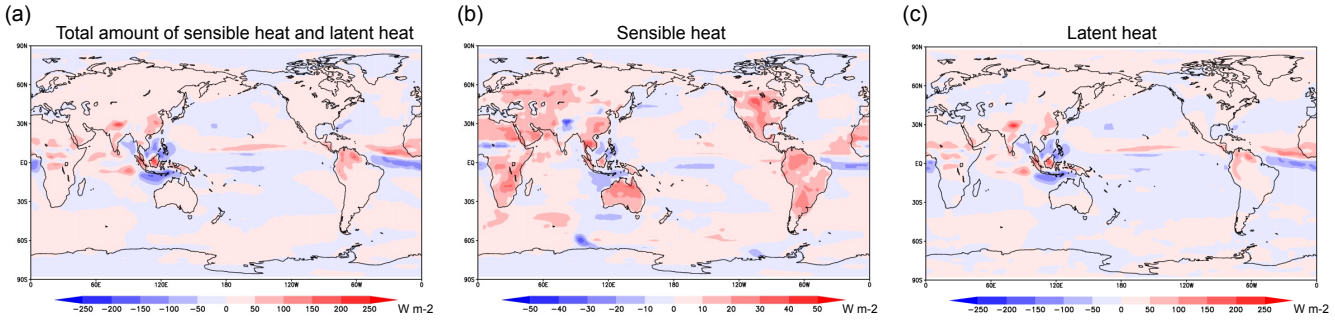

460 **Figure 7.** Anomaly of JJA vertically integrated diabatic heating. (a) The total amount of sensible heat and latent heat, (b) sensible heat, and (c) latent heat. All units are W m^{-2}.